Oxime as a General Photocage for the Design of Visible Light Photoactivatable Fluorophores

Lushun Wang^{a,#}, Shichao Wang^{a,#}, Juan Tang^a, Vanessa B. Espinoza^a, Axel Loredo^a, Zeru Tian^a, R.Bruce Weisman^a, and Han Xiao^{a, c, d*}

- ^a Department of Chemistry, Rice University, 6100 Main Street, Houston, Texas, 77005
- ^b Department of Biosciences, Rice University, 6100 Main Street, Houston, Texas, 77005
- ^c Department of Bioengineering, Rice University, 6100 Main Street, Houston, Texas, 77005
 - * To whom correspondence should be addressed. Email: han.xiao@rice.edu

ABSTRACT

Photoactivatable fluorophores have been widely used for tracking molecular and cellular dynamics with subdiffraction resolution. In this work, we have prepared a series of photoactivatable probes using the oxime moiety as a new class of photolabile caging group in which the photoactivation process is mediated by a highly efficient photodeoximation reaction. Incorporation of the oxime caging group into fluorophores results in loss of fluorescence. Upon light irradiation in the presence of air, the oxime-caged fluorophores are oxidized to their carbonyl derivatives, restoring strong fluorophore fluorescence. To demonstrate the utility of these oxime-caged fluorophores, we have created probes that target different organelles for live-cell confocal imaging. We also carry out photoactivated localization microscopy (PALM) imaging under physiological conditions using low-power light activation in the absence of cytotoxic additives. Our studies show that oximes represent a new class of visible-light photocages that can be widely used for cellular imaging, sensing, and photo-controlled molecular release.

INTRODUCTION

Photoactivatable fluorophores, also known as photocaged fluorophores, are powerful chemical probes for single-particle tracking and localization imaging.^{1–14} Photoactivatable fluorophores are maintained in weakly fluorescent or non-fluorescent dark states via masking by built-in photocaged groups. The photocages can be removed by irradiation with light of appropriate wavelength to restore fluorophore fluorescence. Because they can be activated with high spatiotemporal resolution in complex biological environments, photoactivatable fluorophores have enjoyed a variety of important applications in biological research. These include monitoring of biological processes, detection of biomolecules, and super-resolution biological imaging beyond the diffraction limit.^{15–17}

The center for photoactivatable fluorophore design is the development of photoages or photolabile protecting groups that can alter the emission of conventional fluorescent dyes and can be cleaved upon light irradiation. In exploring the applicability of photocages, researchers have designed photocages based on a variety of different photoactivation mechanisms. 18 Examples of efficient photoactivatable fluorophores include structures based on o-nitrobenzyl or its derivatives, phenacyl, 2-diazoketone, acridinyl, azidophenyl, coumarinyl and o-hydroxynaphthyl moieties. 3,4,6,15,19–37 However, these photocaged dyes are generally characterized by relatively large sizes, poor water solubility, and poor biocompatibility, properties that greatly limit their biological applications.⁴ To minimize side effects resulting from the use of UV light, investigators have developed sensitizer-assisted light-induced cleavage 19,38 and multiphoton activation strategies, 39,40 resulting in efficient photocage cleavage with visible or near-infrared light. The downside of these technologies is the need for a light-capturing sensitizer or an expensive multiphoton light source. In recent years, elegant strategies based on quenching BODIPY dyes have been applied to releasing carboxylic acid and regenerating fluorescence with green light excitation >500 nm. These tactics are promising alternatives for o-nitrobenzyl and other photocaged groups. 13,41-45 Quite recently, a novel light-induced protonation strategy has been employed to prepare a photoactivatable silicon rhodamine derivative. 46 The utility of this fluorophore was successfully demonstrated in livecell single molecule localization microscopy (SMLM) imaging. However, these strategies are limited to certain fluorophore scaffolds.

As a consequence of these difficulties, there is an urgent need for small photocaged moieties that are biocompatible and can be activated with visible light. Because of its small size and weak electron-withdrawing characteristics, the oxime group has been recently employed as a fluorescence quencher that functions by weakening the internal charge

transfer (ICT) process of fluorophores. An ICT-based fluorophore usually contains an electron donor and an electron acceptor, which form a "push-pull" system in the excited state. The introduction of oxime group at the electron acceptor site deactivates the "push-pull" system, blocks the ICT process, and quenches fluorophore fluorescence. Based on this mechanism, carbonyl groups of several fluorophores have been substituted with the oxime group, creating feeble "push-pull" based photocaged fluorophores with weak fluorescence. The resulting oxime-caged fluorophores have been used for the detection of diverse chemicals, including hypochlorous acid/hypochlorite, ^{47–52} phosgene, ^{53,54} ions, ^{55–57} NO₂, ⁵⁸ trichloroisocyanuric acid, ⁵⁹ and organophosphorous nerve agents. ⁶⁰ The basis for most of these detections is a deoximation reaction that occurs in the presence of oxidizing agents. As a result, the technique has rarely been applied to cell imaging.

In this work, we have used the oxime group to prepare photoactivatable fluorophores that undergo a new kind of photoactivation process triggered by visible light (Fig. 1). We find that oxime substitution of the carbonyl group within a variety of fluorophore scaffolds weakens the ICT process, resulting in weak fluorescence. Significantly, excitation with visible light causes the resulting oxime-caged fluorophores to undergo a [2+2] cycloaddition with molecular oxygen, followed by spontaneous dissociation into fluorescent fluorophores with the classic "push-pull" ICT system. This process represents a new photoactivation mechanism in which fluorophore fluorescence is modulated by the photodeoximation reaction. To explore the utility of these oxime-caged photoactivatable fluorophores, we have used

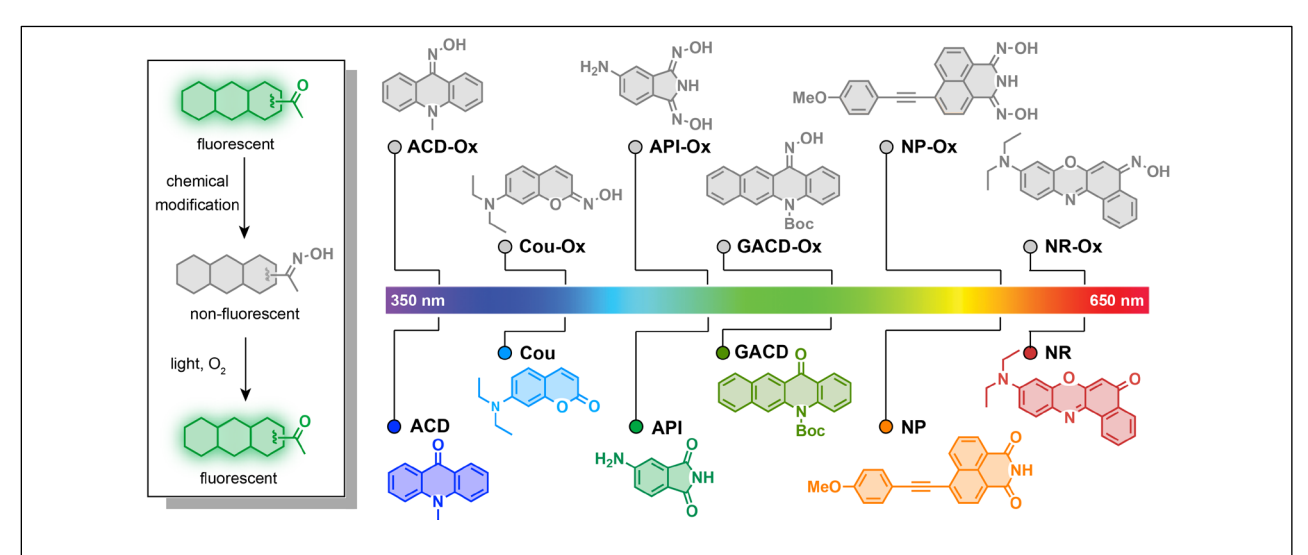


Figure 1. Design of oxime-caged fluorogenic dyes. Oxime substitution at the carbonyl group of fluorophores results in very weak fluorescence via an ICT off mechanism. Upon irradiation with light, the oxime group can be oxidized to its carbonyl derivatives, thus restoring the strong fluorescence of fluorophores.

them for live-cell imaging of different organelles and for super-resolution imaging of proteins of interest in combination with genetically encoded tagging technology.

RESULTS AND DISCUSSION

Synthesis and Characterization of Oxime-caged 10-methylacridin-9(10H)-one

To assess the compatibility of the oxime caging strategy with different fluorophores, we initially synthesized oxime-caged 10-methylacridin-9(10*H*)-one (ACD-Ox, **Fig. 2**) based on a method from the literature.⁶¹ The solution of ACD-Ox in DMSO exhibited three maxima at 262 nm, 300 nm, and 383 nm accompanied by very weak fluorescence (**Fig.** The shorter blue shift of the absorption of ACD-Ox compared to its carbonyl counterpart, 10-methylacridin-9(10*H*)-one (ACD), is likely attributable to the weaker electron-withdrawing ability of oxime relative to the ketone group. The fluorescence quantum yield of ACD-Ox ($\Phi_f = 0.001$) in DMSO is much lower than that of ACD ($\Phi_f = 0.67$), indicating that the oxime should be a suitable caging group (**Table 1**). This also suggests the possibility of oxime modification of the fluorophore for fluorescence quenching, followed by reactivation of the fluorescence by photodeoximation. The shoulder of the absorption spectrum of ACD-Ox extends from 400 nm up to 450 nm,

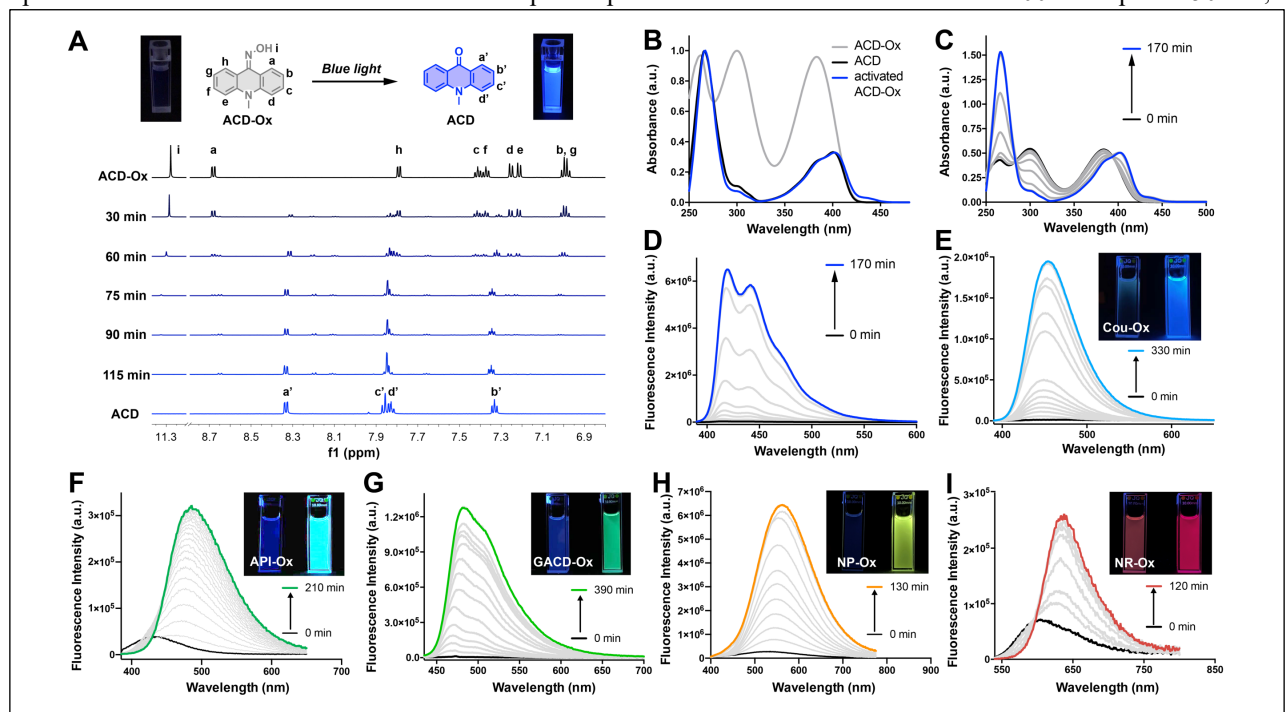


Figure 2. (A) Overlay of ¹HNMR spectra (6.8-11.5 ppm) of ACD-Ox taken at the indicated light irradiation times (430-435 nm, 8.0 μW cm⁻²). (B) Normalized absorbance spectra of ACD, ACD-Ox, and ACD-Ox after photoactivation. (C) Absorbance changes in ACD-Ox after light irradiation for different times (430-435 nm, 7.0 μW cm⁻²). (D) Fluorescence spectra of ACD-Ox after light irradiation for different times (430-435 nm, 7.0 μW cm⁻²). (E-I) Fluorescence spectra of Cou-Ox, API-Ox, GACD-Ox, NP-Ox, and NR-Ox after light irradiation.

suggesting that efficient photoactivation should be achieved using 430 nm light. Gratifyingly, activation of ACD-Ox with blue light (430-435 nm, $7.0 \,\mu\text{W cm}^{-2}$) results in a 400-fold enhancement of fluorescence (**Fig. 2D**). The absorption spectrum of the resulting compound exhibits three maxima at 265 nm, 383 nm, and 401 nm, in good agreement with the absorption peaks of authentic ACD (**Fig. 2B and 2C**).

We used ¹H NMR and ESI-MS analyses to characterize the photoactivation process that occurs in ACD-Ox (**Fig. 2A**). The ¹H NMR spectrum was evaluated at regular time intervals during irradiation of ACD-Ox solution with blue light. Comparison of the ¹H NMR spectrum of ACD-Ox with that of the resulting compound (**Fig. 2A**) reveals the gradual disappearance of signals corresponding to hydroxy and phenyl protons at 11.33, 8.73, 7.84, 7.46, 7.42, 7.30, 7.26, 7.04 ppm, accompanied by the emergence of new signals at 8.35, 7.88, 7.85 and 7.35 ppm. The ¹H NMR spectrum of the resulting product exactly matches that of synthesized ACD. Additional analysis using ESI-MS reveals that the observed m/z 210.0 of the photoactivated compound also corresponds to that ACD (**Fig. S1 and S2**). These results confirm that visible-light photoactivation of ACD-Ox restores the ketone structure of ACD.

Table 1. Photophysical Data of Oxime-Caged and Uncaged Fluorophores

Compoundsa	$\lambda_{abs} (nm)$	ε ^b (*10 ⁴ M ⁻¹ cm ⁻¹)	$\lambda_{em}(nm)$	Φ_{f}^{c}	Turn-on fold
ACD	265, 383, 401	2.33, 0.57, 0.70	420, 441, 473	0.67	-
ACD-Ox	262, 300, 384	0.84, 0.86, 0.83	414, 437, 471	0.001	400
Cou	261, 378	0.95, 2.82	445	0.71	-
Cou-Ox	263, 359	0.30, 1.01	-	0.003	148
API	263, 311, 373	1.06, 0.43, 0.36	479	0.60	-
Ox	265, 297, 342	1.90, 2.98, 0.79	417	0.11	22
GACD	269, 318, 408	3.35, 0.61, 0.22	466, 494	0.44	-
D-Ox	265, 310, 352	1.87, 0.44, 0.13	444	0.006	225
NP	265, 290, 398	2.11, 1.80, 3.52	551	0.32	-
NP-Ox	264, 300, 387	0.46, 0.23, 0.65	526	0.003	26
NR	315, 556	0.92, 4.17	634	0.46	-
NR-Ox	313, 507	0.14, 0.40	600	0.10	6
GACD-Ox-TPP	264, 306, 351	1.15, 0.25, 0.11	439	0.008	90
GACD-Ox-MOR	264, 306, 351	1.52, 0.40, 0.14	452	0.006	108
GACD-Ox-Ts	265, 305, 359	2.63, 0.69, 0.20	453	0.005	184
GACD-Ox-Halo	265, 306, 356	2.63, 0.65, 0.24	455	0.007	103

^a Compounds were dissolved in DMSO (50 μM). ^b ϵ : molar extinction coefficients. ^c Quantum yields were measured using rhodamine B in ethanol or quinine sulfate in 0.5 M H_2SO_4 as the reference.

Extension of the Oxime-Caging Strategy to Other Fluorophores

Encouraged by the outstanding photoactivation properties of ACD-Ox, we extended our design strategy to other commonly used fluorophores. We synthesized a variety of dyes with different scaffolds, as shown in Figure 1. 4-Aminophthalimide-Oxime (API-Ox) was resynthesized as previously reported. 62 For Coumarin-Oxime (Cou-Ox) and Nile Red-Oxime (NR-Ox) syntheses, we used Lawesson's reagent to generate SCou and SNile Red, 11 followed by treatment of the resulting thiocarbonyl compounds with hydroxylamine to yield the oxime moiety (Supporting Information). Tert-butyl-12-(hydroxyamino)benzo[b]acridine-5(12H)-carboxylate (GACD-Ox) was obtained via a synthetic strategy similar to that used for ACD-Ox (Supporting Information). Generation of the oxime caged 4-((4-Methoxyphenyl)ethynyl)-1,8-naphthalimide (NP-Ox) via Sonogashira alkynylation of aryl bromide with 1-ethynyl-4methoxybenzene initially produced 4-methoxyphenyl acetylide in THF/NEt₃ in 85% yield. Subsequent condensation of hydroxylamine with bisnitrile in refluxing ethanol/water generated the desired imidedioxime NP-Ox in moderate yield.⁶³ The photophysical properties and visual fluorescence of these fluorophores were then investigated in DMSO solution at room temperature. As shown in Figure 2 and Table 1, the absorption spectra of oxime-caged fluorophores exhibit blue-shifts compared to their carbonyl analogs (Fig. S3). This can be attributed to the fact that the oxime group has a weaker electron-withdrawing ability than ketone, ester, and amide groups. As expected, the introduction of the oxime group in all selected fluorophores led to dramatic hypsochromic shifts of the emission maxima along with significant reductions in fluorescence quantum yield (Table 1). To evaluate the photoactivation efficiency of the oxime-caged fluorophores, we recorded absorption and emission spectra after different irradiation times (Fig. 2E-I, S4-S9). Upon light irradiation, the fluorescence intensity of Cou-Ox, API-Ox, GACD-Ox, NP-Ox, and NR-Ox exhibited 148-fold, 22-fold, 225-fold, 26-fold, and 6-fold enhancements, respectively. Furthermore, the dramatic shifts of the emission maxima and the good fluorescence quantum yield indicate that API-Ox and NR-Ox can be promising ratiometric fluorescent probes for the detection of bioactive molecules. 47,51,64 These results demonstrate that incorporation of the oxime group into various fluorophores provides a general method for generating photoactivatable dyes.

Mechanism of Oxime-Caged Fluorophore Activation

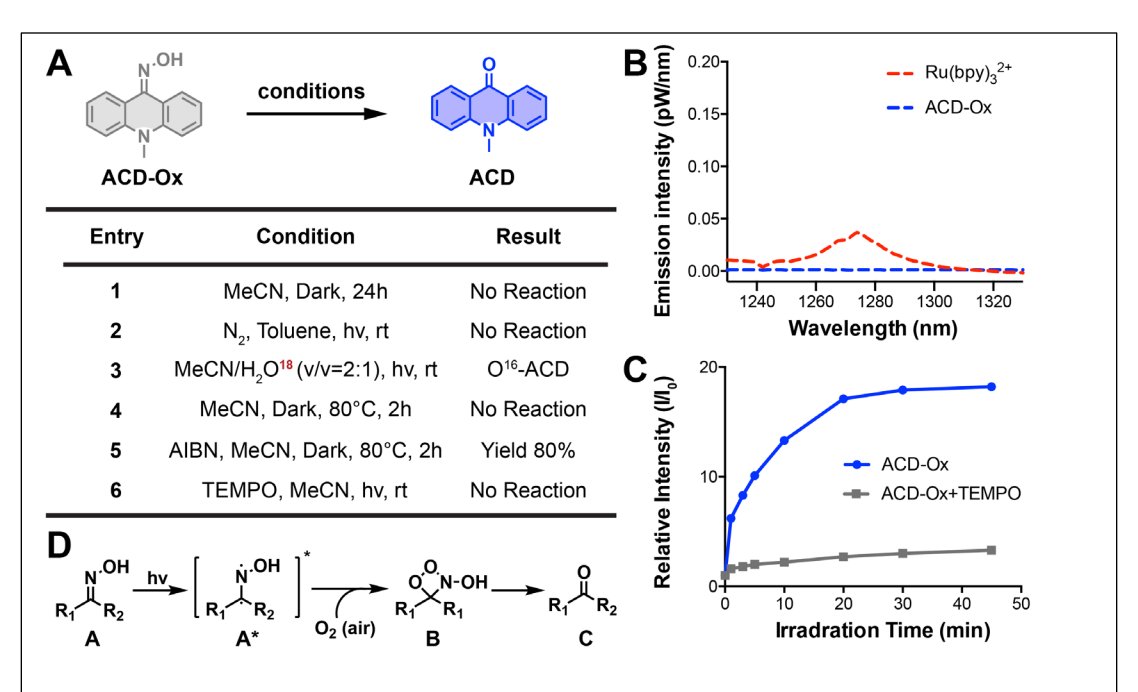


Figure 3. (A) Control experiments for studying the reaction mechanism. (B) Near-IR phosphorescence spectra of singlet oxygen generated by excitation of ACD-Ox and the reference (Ru(bpy)₃²⁺) in oxygen-saturated methanol with 405 nm laser excitation at 25 °C. (C) Fluorescence change in ACD-Ox in the presence and absence of TEMPO under light irradiation. (D)Proposed photoactivation mechanism of oxime-caged fluorophores.

To study the mechanism responsible for fluorescence quenching in oxime caged fluorophores, we performed time-dependent density functional theory (TD-DFT/B3LYP) calculations for the optimized structures of ACD-Ox and ACD in the gas phase. High energy occupied molecular orbitals (HOMOs) and low energy unoccupied molecular orbitals (LUMOs) of ACD-Ox are located throughout the entire ACD-Ox structure, suggesting a very weak intramolecular charge transfer (ICT) effect in this molecule (**Fig. S10**). In contrast, ACD HOMOs and LUMOs are mainly located in the carbonyl area and the benzene conjugated structure, respectively, indicative of a strong ICT effect and robust fluorescence emission under visible light irradiation (**Fig. S10**). These data are consistent with our observations on ACD-Ox and ACD fluorescence.

To further explore the photoactivation mechanism in oxime-caged fluorophores, we carried out several control experiments using ACD-Ox (Supporting Information). First, the light-dependence of ACD-Ox activation was evaluated. No activation product was detected in the dark, confirming that light irradiation is necessary to promote this transformation (**Fig. 3A, entry 1**). Next, the photo-oxidation process was characterized. As shown in Figure 3A, entry 2, no activation product was observed in the absence of oxygen. Isotopic analysis revealed that H₂O was not involved in the photoactivation (**Fig. 3A, entry 3**). Several groups have reported singlet oxygen (${}^{1}O_{2}$)-mediated

oxidation of ketoximes and aldoximes to the corresponding carbonyl compounds and nitric acid. In these cases, the singlet oxygen was generated by irradiation of catalysts (Rose Bengal, Platinum(II) terpyridyl acetylide complex, and potassium poly(heptazine imide)). ⁶⁵⁻⁶⁷ To identify the oxygen species that participate in ACD-Ox photoactivation, we used near-IR phosphorescence to detect the production of singlet oxygen following excitation of ACD-Ox in airsaturated methanol. Singlet oxygen exhibits characteristic phosphorescence at 1275 nm.^{68–71} However, none of our oxime-caged fluorophores showed detectable phosphorescence emission peaks around 1275 nm, indicating that singlet oxygen does not participate in their photoactivation (Fig. 3B and S11). As a positive control, Ru(bpy)₃²⁺ did show a clear structureless emission peak at 1274 nm (Fig. 3B and S11). An alternative mechanism may involve the regeneration of bi-radical intermediates when imine and oxime compounds are exposed to direct irradiation.^{72–75} We investigated this type of radical-mediated mechanism for the photoactivation of oxime-caged fluorophores. Knowing that 2,2,6,6-tetramethylpiperidine-1-oxyl (TEMPO) is a free radical scavenger, we found that the addition of TEMPO dramatically inhibits the photoactivation of oxime-caged fluorophores (Fig. 3A entry 6, and 3C), suggesting the involvement of radical species in the photolysis process. Furthermore, we showed that activation of ACD-Ox occurs in the dark at 80 °C in the presence of the free radical initiator azodiisobutyronitrile (AIBN), producing ACD with an 80% yield (Fig. 3A, entry 5). Taking these experimental data and previous literature into account, ^{72–75} we propose a tentative mechanism for the photoactivation of oxime-caged fluorophores. When irradiated by light, oxime-caged fluorophores are activated to the intermediate bi-radical species A*. Subsequently, oxidation of the radical moiety by dissolved oxygen yields **B**, ⁷² which dissociates to produce the carbonyl compound **C**.

Live-cell confocal imaging using Oxime-caged fluorophores

Having demonstrated the applicability of the oxime-caging strategy to several different fluorophores, we turned our attention to the use of oxime-caged probes for biological imaging. Because of its large increase in fluorescence signal and its low level of cellular autofluorescence, GACD-Ox was employed for live-cell confocal imaging. Prior to live-cell imaging, GACD-Ox was evaluated for stability, membrane permeability, and cell toxicity (**Fig. S12-S14**). Testing in HeLa cells revealed no significant cellular toxicity caused by GACD-Ox (**Fig. S13**). Exposure of living HeLa cells to GACD-Ox (10 μM) showed that the compound has good cell permeability at incubation times no longer than 1 h (**Fig. S14**). In intracellular photoactivation experiments with GACD-Ox, we observed a 22-fold enhancement of

fluorescence, as shown in Video S1, along with very low cellular autofluorescence and negligible background signal (Fig. S14). These results indicate that GACD-Ox is well suited for live-cell imaging.

Fluorescence imaging of organelles in live cells

Organelles, such as the nucleus, endoplasmic recticulum (ER), endosomes, lysosomes, mitochondria, and the Golgi apparatus play significant roles in maintaining subcellular microenvironments. To investigate the properties and functions of these subcellular compartments, investigators have described many elaborately designed probes for fluorescence imaging of organelles.^{76–78} Our study explores the utility of the oxime-caging strategy for organelle-targeted fluorescence imaging.

Synthesis of the organelle-targeted probes commenced with Buchwald - Hartwig cross - coupling amination between commercially available methyl 3-(4-Bromophenyl) propionate 1 and methyl 3-aminonaphthalene-2-carboxylate 2 to provide di-ester 3 in 50% yield (Fig. 4A). Hydrolysis of the di-ester 3 with LiOH was followed by a Friedel - Crafts

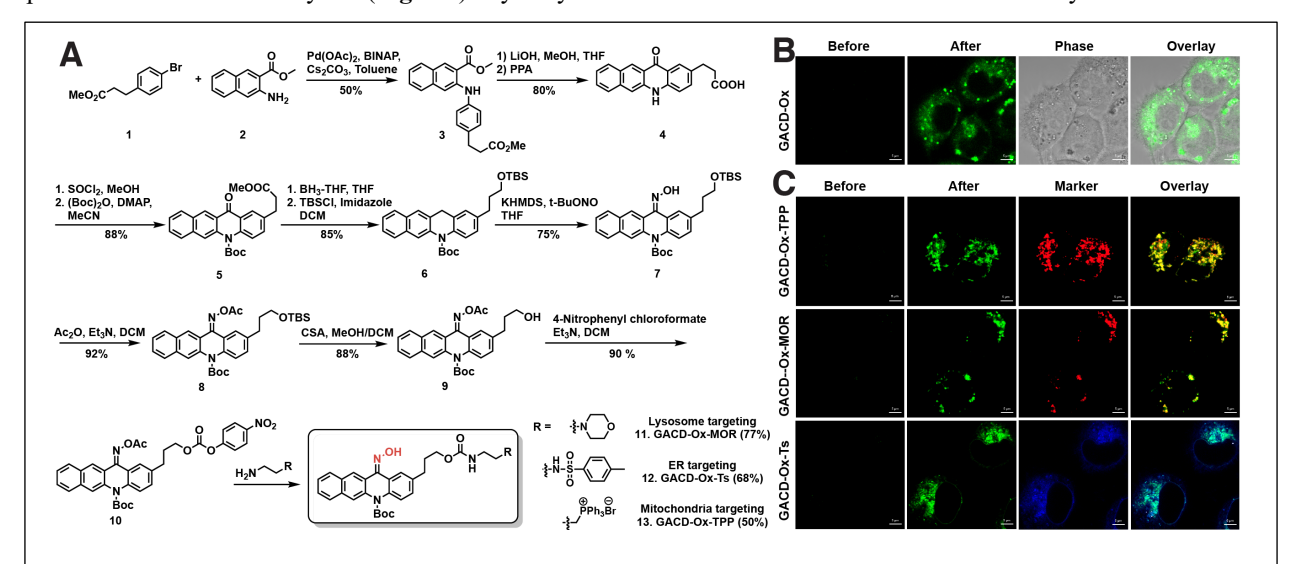


Figure 4. (A) Synthesis of organelle-targeting GACD-Ox fluorogenic fluorophores. (B) Photoactivation of GACD-Ox in A431 cells using 405 nm laser activation. Confocal images were captured before and after 405 nm light activation of GACD-Ox. Scale bar = 5 μm. (C) Photoactivation of organelle-targeting GACD-Ox probes in A431 cells. Confocal images were captured from cells incubated with GACD-Ox-TPP, GACD-Ox-MOR, and GACD-Ox-Ts along with corresponding commercial markers for mitochondria, lysosomes, and endoplasmic reticulum, respectively. Commercial MitoViewTM 633, LysoViewTM 633, and ER-TrackerTM Blue-White DPX were used as markers for mitochondria, lysosomes, and endoplasmic reticulum, respectively. Scale bar = 5 μm.

ring - closing reaction to yield benzo[b]acridin - 12(5H) - one 4.79 Benzo[b]acridin - 12(5H) - one 4 was then transformed into the key intermediate 6 in a 4 step reaction involving (1) esterification of the carboxylic acid with thionyl chloride and methanol; (2) protection of the arylamine with (Boc)₂O; (3) reduction of the ketone moiety with BH₃-THF; (4) protection of the resulting primary alcohol as a TBS ether. Reaction of intermediate 6 with t-BuONO and KHMDS generated the desired oxime as a Z/E isomer mixture in 75% yield.⁶¹ With key intermediates 7 in hand, the oxime hydroxyl moiety was protected with an acetyl group, followed by removal of the TBS group under acidic conditions and activation of the resulting primary hydroxy group as a carbonate ester. The activated GACD-Ox carbonate ester was then functionalized with phenylsulfonamide (GACD-Ox-Ts for endoplasmic reticulum targeting, Table 1 and Fig. 4A), triphenylphosphonium (GACD-Ox-TPP for mitochondrial targeting, Table 1 and Fig. 4A), and morpholine (GACD-Ox-MOR for lysosomal targeting, Table 1 and Fig. 4A). All three organelle-targeting probes exhibited satisfactory stability in the dark, and over 90-fold fluorescence enhancements could be induced by photoactivation in DMSO/PBS (Buffer) (Table 1, Fig. S15-20). Confocal laser scanning microscopy was then used to determine the respective abilities of the three fluorophores to localize to the endoplasmic reticulum, mitochondria, and lysosomes in living cells. Commercial MitoViewTM 633, LysoViewTM 633, and ERTrackerTM Blue-White DPX were used as markers to define the target organelles. Organelle-targeting probes were incubated with A431 cells for 1 h, at which time the excess probe was cleared by washing with PBS. As shown in Figure 4C, negligible fluorescence was observed before photoactivation. Dramatic fluorescence enhancement was then observed upon irradiation with the 405 nm laser. Co-localization experiments confirmed that the fluorescence of GACD-Ox compounds exhibited good co-localization with the respective commercial organelle-specific dyes (Fig. 4C). The high Pearson's correlation coefficients for the organelle markers and GACD-Ox-TPP (γ =0.78), GACD-Ox-MOR (γ =0.90), and GACD-Ox-Ts $(\gamma=0.79)$ indicate that the respective double-staining patterns overlap perfectly. These results verify that the photoactivation of GACD-Ox probes provides an excellent platform for nelle imaging.

Super-Resolution Imaging of Halo-Tag Proteins Using Oxime-Caged Fluorophores

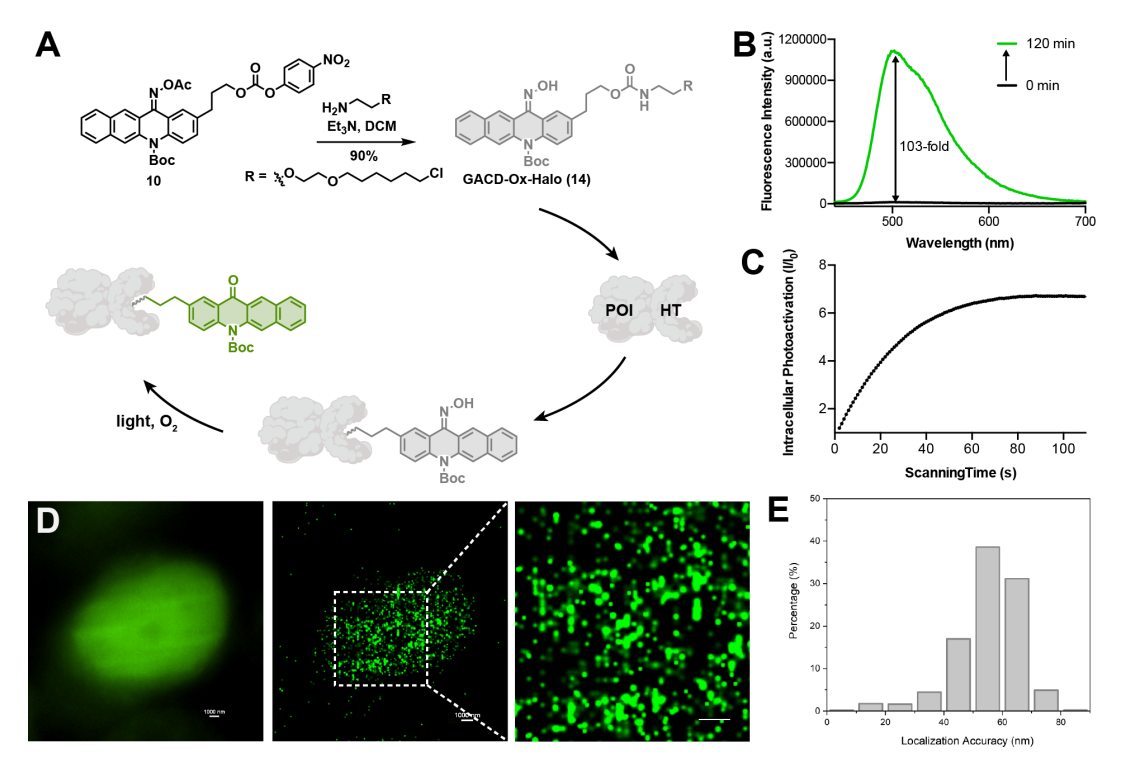


Figure 5. (A) Scheme for labeling the protein of interest (POI) with GACD-Ox-Halo ligand for fluorescence imaging. (B) Fluorescence change of GACD-Ox-Halo in the presence of 430-435 nm light. (C) Intracellular fluorescence change in GACD-Ox-Halo during photoactivation at 405 nm in living CHO-K1 cells. (D) Widefield image and corresponding PALM images of H2B labeled with H2B-HaloTag in CHO-K1 cells. (E) Histogram plot of the localization accuracy of PALM images in (D). Scale bar = 1 μ m.

In recent years, super-resolution microscopy (SRM) techniques have been well developed for biological imaging that overcomes the diffraction limit for light microscopy. ^{80, 81} Photoactivatable or photoswitchable fluorophores have been widely applied to the development of single-molecule localization microscopy (SMLM) techniques, ^{7,8,35,46,82} such as photoactivated localization microscopy (PALM)¹⁶ and stochastic optical reconstruction microscopy (STORM). ¹⁷ The excellent photoactivation properties of GACD-Ox in solution and living cells make it an attractive probe for use in PALM. Accordingly, we synthesized GACD-Ox-Halo (**Fig. 5A**) and evaluated its properties in a PBS buffer/DMSO solution. GACD-Ox-Halo displayed a 103-fold increase in fluorescence upon irradiation with blue light (430-435 nm) (**Table 1, Fig. 5B and Fig. S21**). We next evaluated the suitability of GACD-Ox-Halo for protein super-resolution imaging in live cells. HaloTag labeling technology relies on the formation of a covalent bond between Halo-Tag-fused proteins and a synthetic probe containing a Halo-Tag ligand. Halo-Tag methodology has been used for site-specific labeling of proteins of interest. ^{83–86} Following this line of investigation, we transiently transfected CHO-K1 cells with histone-2B-Halo and stained with GACD-Ox-Halo. Figure 5C shows that irradiation with the 405 nm laser produced

a 7-fold fluorescence enhancement, which was recorded by Video S2, accompanied by a distinct pattern of nuclear

labeling which is further confirmed by the co-incubation of GACD-Ox-Halo with the commercial nuclear dye,

DRAO5 (Fig. S21), as seen with the confocal laser scanning microscope. Following up on this result, we performed

PALM imaging of histone-2B in live CHO-K1 cells. The reconstructed image of histone-2B proteins, obtained from

20,000-30,000 imaging frames, exhibits significant enhancement of resolution (average localization precision of 55.7

nm) compared to the corresponding wide-field image (Fig. 6D and E). This result demonstrates the utility of oxime-

caged fluorophores for PALM imaging under physiological conditions without the addition of toxic enhancers. The

oxime-based fluorophores developed in our work possess an extended functionality for specific labeling of existing

proteins, thus offering great potential for super-resolution imaging in live cells.

CONCLUSION

In summary, we have developed a series of novel photoactivatable probes by incorporating the oxime group into a

large group of fluorophores. The introduction of the oxime into fluorophores produces a reduced ICT effect and

significantly weakened fluorescence. This caging effect can be reversed via a novel photodeoximation reaction

triggered by exposure to air and visible light. We demonstrate the application of these photoactivatable oxime-probes

for confocal imaging of different organelles. Going further, we apply oxime-caged probes to super-resolution imaging

of proteins of interest. We expect that oxime-caged photoactivatable probes and the photodeoximation strategy will

significantly expand strategies for living cell imaging and sensing.

ASSOCIATED CONTENT

Supporting Information

The Supporting Information is available free of charge on the ACS Publication website at DOI: XXXXXXXXXXXXXXX.

Materials and instruments, experimental procedures, details concerning synthesis, NMR, MS, and IR characterization

data, supplemental figures including additional theoretical calculations, photoactivation, stability, and cell imaging

data (PDF)

Video S1: photoactivation of GACD-Ox in HeLa cells (MOV)

Video S2: photoactivation of GACD-Ox -Halo in CHO-K1 cells (MOV)

AUTHOR INFORMATION

Corresponding Author

* E-mail: han.xiao@rice.edu

OCRID

Han Xiao: 0000-0002-4311-971X

Author Contributions

[#]L.W. and S. W. contributed equally.

Notes

The authors declare no competing financial interest.

ACKNOWLEDGMENTS

This work was supported by the Cancer Prevention Research Institute of Texas (CPRIT, RR170014 to H.X.), NIH (R35-GM133706 to H.X., R21-CA255894 to H.X.), U.S. Department of Defense (BC201371 to H.X.), the Robert A. Welch Foundation (C-1970 to H.X. and C-0807 to R.B.W.), the National Science Foundation (CHE-1803066 to R.B.W.), the Hamill Innovation Award (Hamill Foundation), and the John S. Dunn Foundation Collaborative Research Award (Gulf Coast Consortia). H.X. is a Cancer Prevention & Research Institute of Texas (CPRIT) Scholar in Cancer Research.

REFERENCES

- (1) Lavis, L. D.; Chao, T.-Y.; Raines, R. T. Fluorogenic Label for Biomolecular Imaging. ACS Chem. Biol. 2006, 1 (4), 252–260. https://doi.org/10.1021/cb600132m.
- Puliti, D.; Warther, D.; Orange, C.; Specht, A.; Goeldner, M. Small Photoactivatable Molecules for Controlled Fluorescence Activation in Living Cells. Bioorg. Med. Chem. 2011, 19 (3), 1023–1029. https://doi.org/10.1016/j.bmc.2010.07.011.
- Brieke, C.; Rohrbach, F.; Gottschalk, A.; Mayer, G.; Heckel, A. Light-Controlled Tools. Angew. Chem. Int. Ed. 2012, 51 (34), 8446–8476. https://doi.org/10.1002/anie.201202134.
- (4) Li, W.; Zheng, G. Photoactivatable Fluorophores and Techniques for Biological Imaging Applications. Photochem. Photobiol. Sci. 2012, 11 (3), 460. https://doi.org/10.1039/c2pp05342j.
- (5) Chozinski, T. J.; Gagnon, L. A.; Vaughan, J. C. Twinkle, Twinkle Little Star: Photoswitchable Fluorophores for Super-Resolution Imaging. FEBS Lett. 2014, 588 (19), 3603–3612. https://doi.org/10.1016/j.febslet.2014.06.043.
- (6) Grimm, J. B.; English, B. P.; Choi, H.; Muthusamy, A. K.; Mehl, B. P.; Dong, P.; Brown, T. A.; Lippincott-Schwartz, J.; Liu, Z.; Lionnet, T.; Lavis, L. D. Bright Photoactivatable Fluorophores for Single-Molecule Imaging. Nat. Methods 2016, 13 (12), 985–988. https://doi.org/10.1038/nmeth.4034.
- (7) Minoshima, M.; Kikuchi, K. Photostable and Photoswitching Fluorescent Dyes for Super-Resolution Imaging. JBIC J. Biol. Inorg. Chem. 2017, 22 (5), 639–652. https://doi.org/10.1007/s00775-016-1435-y.
- (8) Ye, Z.; Yu, H.; Yang, W.; Zheng, Y.; Li, N.; Bian, H.; Wang, Z.; Liu, Q.; Song, Y.; Zhang, M.; Xiao, Y. Strategy to Lengthen the On-Time of Photochromic Rhodamine Spirolactam for Super-Resolution Photoactivated Localization Microscopy. J. Am. Chem. Soc. 2019, 141 (16), 6527–6536. https://doi.org/10.1021/jacs.8b11369.
- (9) Hauke, S.; von Appen, A.; Quidwai, T.; Ries, J.; Wombacher, R. Specific Protein Labeling with Caged Fluorophores for Dual-Color Imaging and Super-Resolution Microscopy in Living Cells. Chem. Sci. 2017, 8 (1), 559–566. https://doi.org/10.1039/C6SC02088G.
- (10) Raymo, F. M. Photoactivatable Synthetic Dyes for Fluorescence Imaging at the Nanoscale. J. Phys. Chem. Lett. 2012, 3 (17), 2379–2385. https://doi.org/10.1021/jz301021e.

- (11) Tang, J.; Robichaux, M. A.; Wu, K.-L.; Pei, J.; Nguyen, N. T.; Zhou, Y.; Wensel, T. G.; Xiao, H. Single-Atom Fluorescence Switch: A General Approach toward Visible-Light-Activated Dyes for Biological Imaging. J. Am. Chem. Soc. 2019, 141 (37), 14699–14706. https://doi.org/10.1021/jacs.9b06237.
- Dai, S.-Y.; Yang, D. A Visible and Near-Infrared Light Activatable Diazocoumarin Probe for Fluorogenic Protein Labeling in Living Cells. J. Am. Chem. Soc. 2020, 142 (40), 17156–17166. https://doi.org/10.1021/jacs.oco8068.
- (13) Zhang, Y.; Song, K.-H.; Tang, S.; Ravelo, L.; Cusido, J.; Sun, C.; Zhang, H. F.; Raymo, F. M. Far-Red Photoactivatable BODIPYs for the Super-Resolution Imaging of Live Cells. J. Am. Chem. Soc. 2018, 140 (40), 12741–12745. https://doi.org/10.1021/jacs.8b09099.
- (14) Zhang, Y.; Raymo, F. M. Live-Cell Imaging at the Nanoscale with Bioconjugatable and Photoactivatable Fluorophores. Bioconjug. Chem. 2020, 31 (4), 1052–1062. https://doi.org/10.1021/acs.bioconjchem.oco0073.
- (15) Sengupta, P.; van Engelenburg, S. B.; Lippincott-Schwartz, J. Superresolution Imaging of Biological Systems Using Photoactivated Localization Microscopy. Chem. Rev. 2014, 114 (6), 3189–3202. https://doi.org/10.1021/cr400614m.
- (16) Betzig, E.; Patterson, G. H.; Sougrat, R.; Lindwasser, O. W.; Olenych, S.; Bonifacino, J. S.; Davidson, M. W.; Lippincott-Schwartz, J.; Hess, H. F. Imaging Intracellular Fluorescent Proteins at Nanometer Resolution. Science 2006, 313 (5793), 1642–1645. https://doi.org/10.1126/science.1127344.
- (17) Rust, M. J.; Bates, M.; Zhuang, X. Sub-Diffraction-Limit Imaging by Stochastic Optical Reconstruction Microscopy (STORM). Nat. Methods 2006, 3 (10), 793–796. https://doi.org/10.1038/nmeth929.
- (18) Abou Nakad, E.; Chaud, J.; Morville, C.; Bolze, F.; Specht, A. Monitoring of Uncaging Processes by Designing Photolytical Reactions. Photochem. Photobiol. Sci. 2020, 19 (9), 1122–1133. https://doi.org/10.1039/DoPPo0169D.
- (19) Nani, R. R.; Gorka, A. P.; Nagaya, T.; Kobayashi, H.; Schnermann, M. J. Near-IR Light-Mediated Cleavage of Antibody–Drug Conjugates Using Cyanine Photocages. Angew. Chem. 2015, 127 (46), 13839–13842. https://doi.org/10.1002/ange.201507391.
- Belov, V. N.; Wurm, C. A.; Boyarskiy, V. P.; Jakobs, S.; Hell, S. W. Rhodamines NN: A Novel Class of Caged Fluorescent Dyes. Angew. Chem. Int. Ed. 2010, 49 (20), 3520–3523. https://doi.org/10.1002/anie.201000150.
- (21) Krafft, G. A.; Sutton, W. Randall.; Cummings, R. T. Photoactivable Fluorophores. 3. Synthesis and Photoactivation of Fluorogenic Difunctionalized Fluoresceins. J. Am. Chem. Soc. 1988, 110 (1), 301–303. https://doi.org/10.1021/ja00209a055.
- (22) Givens, R. S.; Matuszewski, B. Photochemistry of Phosphate Esters: An Efficient Method for the Generation of Electrophiles. 2.
- Olson, J. P.; Banghart, M. R.; Sabatini, B. L.; Ellis-Davies, G. C. R. Spectral Evolution of a Photochemical Protecting Group for Orthogonal Two-Color Uncaging with Visible Light. J. Am. Chem. Soc. 2013, 135 (42), 15948–15954. https://doi.org/10.1021/ja408225k.
- (24) Antony, L. A. P.; Slanina, T.; Šebej, P.; Šolomek, T.; Klán, P. Fluorescein Analogue Xanthene-9-Carboxylic Acid: A Transition-Metal-Free CO Releasing Molecule Activated by Green Light. Org. Lett. 2013, 15 (17), 4552–4555. https://doi.org/10.1021/014021089.
- (25) Sharma, R.; Knoll, J. D.; Martin, P. D.; Podgorski, I.; Turro, C.; Kodanko, J. J. Ruthenium Tris(2-Pyridylmethyl)Amine as an Effective Photocaging Group for Nitriles. Inorg. Chem. 2014, 53 (7), 3272–3274. https://doi.org/10.1021/ic500299s.
- (26) Arumugam, S.; Popik, V. V. Photochemical Generation and the Reactivity of o -Naphthoquinone Methides in Aqueous Solutions. J. Am. Chem. Soc. 2009, 131 (33), 11892–11899. https://doi.org/10.1021/ja9031924.
- Zhang, Y.; Song, K.-H.; Tang, S.; Ravelo, L.; Cusido, J.; Sun, C.; Zhang, H. F.; Raymo, F. M. Far-Red Photoactivatable BODIPYs for the Super-Resolution Imaging of Live Cells. J. Am. Chem. Soc. 2018, 140 (40), 12741–12745. https://doi.org/10.1021/jacs.8b09099.
- Zou, Z.; Luo, Z.; Xu, X.; Yang, S.; Qing, Z.; Liu, J.; Yang, R. Photoactivatable Fluorescent Probes for Spatiotemporal-Controlled Biosensing and Imaging. TrAC Trends Anal. Chem. 2020, 125, 115811. https://doi.org/10.1016/j.trac.2020.115811.
- (29) Halabi, E. A.; Thiel, Z.; Trapp, N.; Pinotsi, D.; Rivera-Fuentes, P. A Photoactivatable Probe for Super-Resolution Imaging of Enzymatic Activity in Live Cells. J. Am. Chem. Soc. 2017, 139 (37), 13200–13207. https://doi.org/10.1021/jacs.7b07748.

- (30) Klötzner, D.-P.; Klehs, K.; Heilemann, M.; Heckel, A. A New Photoactivatable Near-Infrared-Emitting QCy7 Fluorophore for Single-Molecule Super-Resolution Microscopy. Chem. Commun. 2017, 53 (71), 9874–9877. https://doi.org/10.1039/C7CC04996J.
- (31) Lord, S. J.; Conley, N. R.; Lee, H. D.; Samuel, R.; Liu, N.; Twieg, R. J.; Moerner, W. E. A Photoactivatable Push–Pull Fluorophore for Single-Molecule Imaging in Live Cells. J. Am. Chem. Soc. 2008, 130 (29), 9204–9205. https://doi.org/10.1021/ja802883k.
- (32) Lee, H. D.; Lord, S. J.; Iwanaga, S.; Zhan, K.; Xie, H.; Williams, J. C.; Wang, H.; Bowman, G. R.; Goley, E. D.; Shapiro, L.; Twieg, R. J.; Rao, J.; Moerner, W. E. Superresolution Imaging of Targeted Proteins in Fixed and Living Cells Using Photoactivatable Organic Fluorophores. 3.
- (33) Grimm, J. B.; Klein, T.; Kopek, B. G.; Shtengel, G.; Hess, H. F.; Sauer, M.; Lavis, L. D. Synthesis of a Far-Red Photoactivatable Silicon-Containing Rhodamine for Super-Resolution Microscopy. Angew. Chem. Int. Ed. 2016, 55 (5), 1723–1727. https://doi.org/10.1002/anie.201509649.
- Wysocki, L. M.; Grimm, J. B.; Tkachuk, A. N.; Brown, T. A.; Betzig, E.; Lavis, L. D. Facile and General Synthesis of Photoactivatable Xanthene Dyes. Angew. Chem. Int. Ed. 2011, 50 (47), 11206–11209. https://doi.org/10.1002/anie.201104571.
- (35) Hauke, S. Specific Protein Labeling with Caged Fluorophores for Dual-Color Imaging and Super-Resolution Microscopy in Living Cells. Chem. Sci. 2017, 8.
- (36) Zhang, Y.; Swaminathan, S.; Tang, S.; Garcia-Amoros, J.; Boulina, M.; Captain, B.; Baker, J. D. Photoactivatable BODIPYs Designed To Monitor the Dynamics of Supramolecular Nanocarriers. J Am Chem Soc 2015, 11.
- (37) Anzalone, A. V.; Chen, Z.; Cornish, V. W. Synthesis of Photoactivatable Azido-Acyl Caged Oxazine Fluorophores for Live-Cell Imaging. Chem. Commun. 2016, 52 (60), 9442–9445. https://doi.org/10.1039/C6CC04882J.
- (38) Atilgan, A.; Tanriverdi Eçik, E.; Guliyev, R.; Uyar, T. B.; Erbas-Cakmak, S.; Akkaya, E. U. Near-IR-Triggered, Remote-Controlled Release of Metal Ions: A Novel Strategy for Caged Ions. Angew. Chem. Int. Ed. 2014, 53 (40), 10678–10681. https://doi.org/10.1002/anie.201405462.
- Brown, E. B.; Shear, J. B.; Adams, S. R.; Tsien, R. Y.; Webb, W. W. Photolysis of Caged Calcium in Femtoliter Volumes Using Two-Photon Excitation. Biophys. J. 1999, 76 (1 Pt 1), 489–499.
- (40) Tran, C.; Gallavardin, T.; Petit, M.; Slimi, R.; Dhimane, H.; Blanchard-Desce, M.; Acher, F. C.; Ogden, D.; Dalko, P. I. Two-Photon "Caging" Groups: Effect of Position Isomery on the Photorelease Properties of Aminoquinoline-Derived Photolabile Protecting Groups. Org. Lett. 2015, 17 (3), 402–405. https://doi.org/10.1021/015035035.
- (41) Goswami, P. P.; Syed, A.; Beck, C. L.; Albright, T. R.; Mahoney, K. M.; Unash, R.; Smith, E. A.; Winter, A. H. BODIPY-Derived Photoremovable Protecting Groups Unmasked with Green Light. J. Am. Chem. Soc. 2015, 137 (11), 3783–3786. https://doi.org/10.1021/jacs.5b01297.
- (42) Shrestha, P.; Dissanayake, K. C.; Gehrmann, E. J.; Wijesooriya, C. S.; Mukhopadhyay, A.; Smith, E. A.; Winter, A. H. Efficient Far-Red/Near-IR Absorbing BODIPY Photocages by Blocking Unproductive Conical Intersections. J. Am. Chem. Soc. 2020, 142 (36), 15505–15512. https://doi.org/10.1021/jacs.oco7139.
- Rubinstein, N.; Liu, P.; Miller, E. W.; Weinstain, R. Meso-Methylhydroxy BODIPY: A Scaffold for Photo-Labile Protecting Groups. Chem. Commun. 2015, 51 (29), 6369–6372. https://doi.org/10.1039/C5CC00550G.
- Slanina, T.; Shrestha, P.; Palao, E.; Kand, D.; Peterson, J. A.; Dutton, A. S.; Rubinstein, N.; Weinstain, R.; Winter, A. H.; Klán, P. In Search of the Perfect Photocage: Structure–Reactivity Relationships in Meso-Methyl BODIPY Photoremovable Protecting Groups. J. Am. Chem. Soc. 2017, 139 (42), 15168–15175. https://doi.org/10.1021/jacs.7b08532.
- (45) Peterson, J. A.; Wijesooriya, C.; Gehrmann, E. J.; Mahoney, K. M.; Goswami, P. P.; Albright, T. R.; Syed, A.; Dutton, A. S.; Smith, E. A.; Winter, A. H. Family of BODIPY Photocages Cleaved by Single Photons of Visible/Near-Infrared Light. J. Am. Chem. Soc. 2018, 140 (23), 7343–7346. https://doi.org/10.1021/jacs.8b04040.
- (46) Frei, M. S.; Hoess, P.; Lampe, M.; Nijmeijer, B.; Kueblbeck, M.; Ellenberg, J.; Wadepohl, H.; Ries, J.; Pitsch, S.; Reymond, L.; Johnsson, K. Photoactivation of Silicon Rhodamines via a Light-Induced Protonation. Nat. Commun. 2019, 10 (1), 4580. https://doi.org/10.1038/s41467-019-12480-3.

- Lin, W.; Long, L.; Chen, B.; Tan, W. A Ratiometric Fluorescent Probe for Hypochlorite Based on a Deoximation Reaction. Chem. Eur. J. 2009, 15 (10), 2305–2309. https://doi.org/10.1002/chem.200802054.
- (48) Cheng, X.; Jia, H.; Long, T.; Feng, J.; Qin, J.; Li, Z. A "Turn-on" Fluorescent Probe for Hypochlorous Acid: Convenient Synthesis, Good Sensing Performance, and a New Design Strategy by the Removal of CN Isomerization. Chem. Commun. 2011, 47 (43), 11978–11980. https://doi.org/10.1039/C1CC15214A.
- (49) Emrullahoğlu, M.; Üçüncü, M.; Karakuş, E. A BODIPY Aldoxime-Based Chemodosimeter for Highly Selective and Rapid Detection of Hypochlorous Acid. Chem. Commun. 2013, 49 (71), 7836–7838. https://doi.org/10.1039/C3CC44463E.
- (50) Ma, C.; Zhong, G.; Zhao, Y.; Zhang, P.; Fu, Y.; Shen, B. Recent Development of Synthetic Probes for Detection of Hypochlorous Acid/Hypochlorite. Spectrochim. Acta. A. Mol. Biomol. Spectrosc. 2020, 240, 118545. https://doi.org/10.1016/j.saa.2020.118545.
- (51) Kang, J.; Huo, F.; Yue, Y.; Wen, Y.; Chao, J.; Zhang, Y.; Yin, C. A Solvent Depend on Ratiometric Fluorescent Probe for Hypochlorous Acid and Its Application in Living Cells. Dyes Pigments 2017, 136, 852–858. https://doi.org/10.1016/j.dyepig.2016.09.048.
- Wang, L.; Liu, J.; Zhang, H.; Guo, W. Discrimination between Cancerous and Normal Cells/Tissues Enabled by a near-Infrared Fluorescent HClO Probe. Sens. Actuators B Chem. 2021, 334, 129602. https://doi.org/10.1016/j.snb.2021.129602.
- Ma, B.; Wang, X.; Gao, S.; Qi, L.; Xu, Y.; Yang, J.; Zuo, G. Iridium(III) Complex-Based Phosphorescent Probe for Rapid, Specific, and Sensitive Detection of Phosgene. Dyes Pigments 2020, 177, 108279. https://doi.org/10.1016/j.dyepig.2020.108279.
- (54) Kim, T.-I.; Hwang, B.; Bouffard, J.; Kim, Y. Instantaneous Colorimetric and Fluorogenic Detection of Phosgene with a Meso-Oxime-BODIPY. Anal. Chem. 2017, 89 (23), 12837–12842. https://doi.org/10.1021/acs.analchem.7b03316.
- (55) Chen, K.; Bats, J. W.; Schmittel, M. Iridium-Based Lab-on-a-Molecule for Hg 2+ and ClO with Two Distinct Light-Up Emissions. Inorg. Chem. 2013, 52 (22), 12863–12865. https://doi.org/10.1021/ic401983h.
- (56) Balamurugan, A.; Lee, H. Single Molecular Probe for Multiple Analyte Sensing: Efficient and Selective Detection of Mercury and Fluoride Ions. Sens. Actuators B Chem. 2015, 216, 80–85. https://doi.org/10.1016/j.snb.2015.04.026.
- (57) Sivamani, J.; Sadhasivam, V.; Siva, A. Aldoxime Based Biphenyl-Azo Derivative for Self-Assembly, Chemosensor (Hg2+/F–) and Bioimaging Studies. Sens. Actuators B Chem. 2017, 246, 108–117. https://doi.org/10.1016/j.snb.2017.02.068.
- (58) Juárez, L. A.; Costero, A. M.; Parra, M.; Gil, S.; Ródenas, J.; Sancenón, F.; Martínez-Máñez, R. Biphenyl Derivatives Containing Trimethylsilyl Benzyl Ether or Oxime Groups as Probes for NO2 Detection. RSC Adv. 2016, 6 (49), 43719–43723. https://doi.org/10.1039/C6RA02222G.
- (59) Lee, S. K.; Choi, M. G.; Chang, S.-K. Signaling of Chloramine: A Fluorescent Probe for Trichloroisocyanuric Acid Based on Deoximation of a Coumarin Oxime. Tetrahedron Lett. 2014, 55 (51), 7047–7050. https://doi.org/10.1016/j.tetlet.2014.10.132.
- (60) Lee, H.; Kim, H.-J. Novel Fluorescent Probe for the Selective Detection of Organophosphorous Nerve Agents through a Cascade Reaction from Oxime to Nitrile via Isoxazole. Tetrahedron 2014, 70 (18), 2966–2970. https://doi.org/10.1016/j.tet.2014.03.026.
- (61) Tokuyama, H.; Cho, H.; Iwama, Y.; Noro, T.; Okano, K. Formation of Xanthone Oxime and Related Compounds Using a Combination of Tert-Butyl Nitrite and Potassium Hexamethyldisilazide. HETEROCYCLES 2014, 88 (2), 1433. https://doi.org/10.3987/COM-13-S(S)110.
- (62) Carboni, M.; Abney, C. W.; Taylor-Pashow, K. M. L.; Vivero-Escoto, J. L.; Lin, W. Uranium Sorption with Functionalized Mesoporous Carbon Materials. Ind. Eng. Chem. Res. 2013, 52 (43), 15187–15197. https://doi.org/10.1021/ie402646r.
- (63) Grant, C. D.; Kang, S. O.; Hay, B. P. Synthesis of a Hydrophilic Naphthalimidedioxime. J. Org. Chem. 2013, 78 (15), 7735–7740. https://doi.org/10.1021/j04009386.

- Jiang, Q.; Wang, Z.; Li, M.; Song, J.; Yang, Y.; Xu, X.; Xu, H.; Wang, S. A Novel Nopinone-Based Fluorescent Probe for Colorimetric and Ratiometric Detection of Hypochlorite and Its Applications in Water Samples and Living Cells. The Analyst 2020, 145 (3), 1033–1040. https://doi.org/10.1039/C9AN01981B.
- (65) Wamser, C. C.; Herring, J. W. Photooxidation of Benzophenone Oxime and Derivatives. J. Org. Chem. 1976, 41 (8), 1476–1477. https://doi.org/10.1021/j000870a045.
- (66) Yang, Y.; Zhang, D.; Wu, L.-Z.; Chen, B.; Zhang, L.-P.; Tung, C.-H. Photosensitized Oxidative Deprotection of Oximes to Their Corresponding Carbonyl Compounds by Platinum(II) Terpyridyl Acetylide Complex. J. Org. Chem. 2004, 69 (14), 4788–4791. https://doi.org/10.1021/j0049895e.
- (67) Savateev, A.; Tarakina, N. V.; Strauss, V.; Hussain, T.; Brummelhuis, K. ten; Vadillo, J. M. S.; Markushyna, Y.; Mazzanti, S.; Tyutyunnik, A. P.; Walczak, R.; Oschatz, M.; Guldi, D. M.; Karton, A.; Antonietti, M. Potassium Poly(Heptazine Imide): Transition Metal-Free Solid-State Triplet Sensitizer in Cascade Energy Transfer and [3+2]-Cycloadditions. Angew. Chem. Int. Ed. 2020, 59 (35), 15061–15068. https://doi.org/10.1002/anie.202004747.
- (68) Tsuchiya, T.; Kikuchi, A.; Oguchi-Fujiyama, N.; Miyazawa, K.; Yagi, M. Photoexcited Triplet States of UV-B Absorbers: Ethylhexyl Triazone and Diethylhexylbutamido Triazone. Photochem. Photobiol. Sci. 2015, 14 (4), 807–814. https://doi.org/10.1039/C4PP00373J.
- (69) Fukuchi, S.; Yagi, M.; Oguchi-Fujiyama, N.; Kang, J.; Kikuchi, A. A Novel Characteristic of Salicylate UV Absorbers: Suppression of Diethylhexyl 2,6-Naphthalate (Corapan TQ)-Photosensitized Singlet Oxygen Generation. Photochem. Photobiol. Sci. 2019, 18 (6), 1556–1564. https://doi.org/10.1039/C9PP00104B.
- (70) Kitasaka, S.; Yagi, M.; Kikuchi, A. Suppression of Menthyl Anthranilate (UV-A Sunscreen)-Sensitized Singlet Oxygen Generation by Trolox and α-Tocopherol. Photochem. Photobiol. Sci. 2020, 19 (7), 913–919. https://doi.org/10.1039/DoPP00023J.
- (71) Lin, C.-W.; Bachilo, S. M.; Weisman, R. B. Delayed Fluorescence from Carbon Nanotubes through Singlet Oxygen-Sensitized Triplet Excitons. J. Am. Chem. Soc. 2020, 142 (50), 21189–21196. https://doi.org/10.1021/jacs.oc10557.
- (72) Toshima, N.; Hirai, H. Photochemical Oxidation of Imines. Tetrahedron Lett. 1970, 11 (6), 433–436. https://doi.org/10.1016/0040-4039(70)80067-3.
- (73) Castro, C.; Dixon, M.; Erden, I.; Ergonenc, P.; Keeffe, J. R.; Sukhovitsky, A. Dye-Sensitized Photooxygenation of the Carbon-Nitrogen Double Bond. J. Org. Chem. 1989, 54 (15), 3732–3738. https://doi.org/10.1021/j000276a042.
- Li, H.; Jing, X.; Shi, Y.; Yu, L. Autocatalytic Deoximation Reactions Driven by Visible Light. React. Chem. Eng. 2021, 6 (1), 119–124. https://doi.org/10.1039/DoRE00333F.
- (75) Becker, M. R.; Richardson, A. D.; Schindler, C. S. Functionalized Azetidines via Visible Light-Enabled Aza Paternò-Büchi Reactions. Nat. Commun. 2019, 10 (1), 5095. https://doi.org/10.1038/s41467-019-13072-x.
- (76) Gao, P.; Pan, W.; Li, N.; Tang, B. Fluorescent Probes for Organelle-Targeted Bioactive Species Imaging. Chem. Sci. 2019, 10 (24), 6035–6071. https://doi.org/10.1039/C9SC01652J.
- (77) Lukinavičius, G.; Reymond, L.; Umezawa, K.; Sallin, O.; D'Este, E.; Göttfert, F.; Ta, H.; Hell, S. W.; Urano, Y.; Johnsson, K. Fluorogenic Probes for Multicolor Imaging in Living Cells. J. Am. Chem. Soc. 2016, 138 (30), 9365–9368. https://doi.org/10.1021/jacs.6b04782.
- (78) Ye, S.; Zhang, H.; Fei, J.; Wolstenholme, C. H.; Zhang, X. A General Strategy to Control Viscosity Sensitivity of Molecular Rotor-Based Fluorophores. Angew. Chem. Int. Ed. 2021, 60 (3), 1339–1346. https://doi.org/10.1002/anie.20201108.
- (79) Sungwienwong, I.; Ferrie, J. J.; Jun, J. V.; Liu, C.; Barrett, T. M.; Hostetler, Z. M.; Ieda, N.; Hendricks, A.; Muthusamy, A. K.; Kohli, R. M.; Chenoweth, D. M.; Petersson, G. A.; Petersson, E. J. Improving the Fluorescent Probe Acridonylalanine through a Combination of Theory and Experiment. J. Phys. Org. Chem. 2018, 31 (8), e3813. https://doi.org/10.1002/poc.3813.
- (80) Sydor, A. M.; Czymmek, K. J.; Puchner, E. M.; Mennella, V. Super-Resolution Microscopy: From Single Molecules to Supramolecular Assemblies. Trends Cell Biol. 2015, 25 (12), 730–748. https://doi.org/10.1016/j.tcb.2015.10.004.
- (81) Hell, S. W. Nanoscopy with Focused Light (Nobel Lecture). Angew. Chem. Int. Ed. 2015, 54 (28), 8054–8066. https://doi.org/10.1002/anie.201504181.

- (82) Tang, J.; Zhang, M.; Yin, H.-Y.; Jing, J.; Xie, D.; Xu, P.; Zhang, J.-L. A Photoactivatable Znsalen Complex for Super-Resolution Imaging of Mitochondria in Living Cells. Chem. Commun. 2016, 52 (77), 11583–11586. https://doi.org/10.1039/C6CC06531G.
- (83) England, C. G.; Luo, H.; Cai, W. HaloTag Technology: A Versatile Platform for Biomedical Applications. Bioconjug. Chem. 2015, 26 (6), 975–986. https://doi.org/10.1021/acs.bioconjchem.5b00191.
- (84) Los, G. V.; Encell, L. P.; McDougall, M. G.; Hartzell, D. D.; Karassina, N.; Zimprich, C.; Wood, M. G.; Learish, R.; Ohana, R. F.; Urh, M.; Simpson, D.; Mendez, J.; Zimmerman, K.; Otto, P.; Vidugiris, G.; Zhu, J.; Darzins, A.; Klaubert, D. H.; Bulleit, R. F.; Wood, K. V. HaloTag: A Novel Protein Labeling Technology for Cell Imaging and Protein Analysis. ACS Chem. Biol. 2008, 3 (6), 373–382. https://doi.org/10.1021/cb800025k.
- (85) Liu, Y.; Miao, K.; Dunham, N. P.; Liu, H.; Fares, M.; Boal, A. K.; Li, X.; Zhang, X. The Cation– π Interaction Enables a Halo-Tag Fluorogenic Probe for Fast No-Wash Live Cell Imaging and Gel-Free Protein Quantification. Biochemistry 2017, 56 (11), 1585–1595. https://doi.org/10.1021/acs.biochem.7b00056.
- Liu, Y.; Miao, K.; Li, Y.; Fares, M.; Chen, S.; Zhang, X. A HaloTag-Based Multicolor Fluorogenic Sensor Visualizes and Quantifies Proteome Stress in Live Cells Using Solvatochromic and Molecular Rotor-Based Fluorophores. Biochemistry 2018, 57 (31), 4663–4674. https://doi.org/10.1021/acs.biochem.8bo0135.